HHS Public Access

Author manuscript

Brain Imaging Behav. Author manuscript; available in PMC 2023 June 01.

Published in final edited form as:

Brain Imaging Behav. 2023 June ; 17(3): 306–319. doi:10.1007/s11682-023-00764-8.

Hypo- and Hyper-perfusion in MCI and AD Identified by Different ASL MRI Sequences

Aldo Camargo, Ph.D.[1], **Ze Wang, Ph.D.**[1,#],

Alzheimer's Disease Neuroimaging Initiative*

[1]Department of Diagnostic Radiology & Nuclear Medicine, University of Maryland School of Medicine, Baltimore, Maryland, USA.

Abstract

Arterial spin labeling (ASL) perfusion MRI has been increasingly used in Alzheimer's Disease (AD) research. Because ASL MRI sequences differ greatly in terms of arterial blood signal preparations and data acquisition strategies, both leading to a large difference of signal-to-noise ratio (SNR), it is of great translational importance to compare the several widely used ASL MRI sequences regarding sensitivity of ASL measured cerebral blood flow (CBF) for detecting the between-group difference across the AD continuum. To this end, this study compared three ASL MRI sequences in AD research, including the 2D Pulsed ASL (PASL), 3D Background Suppressed (BS) PASL, and 3D BS Pseudo-Continuous ASL (PCASL). We used data from 100 healthy and cognitively normal elderly control (NC) subjects, 75 patients with mild cognitive impairment (MCI), and 57 Alzheimer's disease (AD) subjects from the AD neuroimaging initiative (ADNI). Both cross-sectional perfusion difference and perfusion versus clinical assessment correlations were examined. The major findings included: 3D PCASL sequence identified stronger patient versus control CBF/rCBF differences than 2D PASL and 3D PCASL; MCI showed reduced CBF and CBF redistribution; CBF in orbito-frontal cortex presents a U-shape change pattern from normal aging to MCI and to AD; 3D PCASL identified negative rCBF to memory correlation while 2D PASL showed positive correlation.

*Data used in the preparation of this article were obtained from the Alzheimer's Disease Neuroimaging Initiative (ADNI) database (adni.loni.usc.edu). As such, the investigators within the ADNI contributed to the design and implementation of ADNI and/or provided data but did not participate in the analysis or writing of this report. A complete listing of ADNI investigators can be found at: http://adni.loni.usc.edu/wp-content/uploads/how_to_apply/ADNI_Acknowledgement_List.pdf

#Correspondence: Ze Wang (ze.wang@som.umaryland.edu), HSF III Room 1173, 670 W Baltimore St, MD 21201, Phone: 410-706-2797.

AUTHOR CONTRIBUTIONS

AC downloaded the data, analyzed, and interpreted the data, and wrote the initial version of the manuscript. ZW designed the study, interpreted the results, wrote the manuscript.

Competing interest

The authors declare that the research was conducted in the absence of any commercial or financial relationships that could be construed as a potential conflict of interest.

Ethical Approval

Subject recruitment and data acquisition were approved by the Internal Review Boards for the parent ADNI project. All human subjects provided written consent forms before participating the ADNI study. Data re-analysis for this study was approved by Internal Review Board of University of Maryland Baltimore.

Keywords

Alzheimer's disease; cerebral blood flow; 2D PASL; 3D PCASL; 3D PASL

INTRODUCTION

Alzheimer's disease (AD) is the most common type of dementia and the 6th leading cause of death in the United States (Solis Jr et al., 2020). AD has been characterized by amyloid-beta deposition and tau pathology, but these pathological changes often do not lead to clinical symptoms are insensitive to disease progression. Functional brain measures such as cerebral blood flow (CBF) are necessary to understand the AD pathology versus symptom discrepancy. CBF is a key physiological index that reflects cerebral metabolism associated with regional functional activity(Baron et al., 1982; J. A. Detre et al., 2012; DeWitt et al., 1988; Furlow et al., 1983; Liu et al., 2004; Musiek et al., 2012; Raichle, 1998; Vestergaard et al., 2016). CBF has long been investigated as a regional brain marker for brain function(J. A. Detre et al., 2012; Detre et al., 2009) and has been increasingly studied in AD (Alsop et al., 2008; Alsop et al., 2010; Alsop et al., 2000; Wang, 2014; Wolk & Detre, 2012; Xu et al., 2010; Ze Wang, 2013).

Arterial Spin Labeling (ASL) MRI is a completely noninvasive technique for measuring cerebral blood flow (CBF) (Detre et al., 1992). Using the magnetically labeled arterial blood as the endogenous tracer, ASL MRI measures the perfusion signal through the tissue signal changes induced by the labeled arterial blood water that exchanged with tissue water. To control the background tissue signal, the arterial spin labeling radiofrequency pulses are phase modulated to have zero net effects on the arterial blood water magnetization. The control image acquired using this arterial blood magnetization untagged sequence is considered the baseline image. The perfusion-weighted signal is then extracted from the difference between the control and label images (John A Detre et al., 2012; Luis Hernandez-Garcia, 2022; Wang, 2022). The quantitative CBF can be calculated from the ratio between the weighted perfusion signal and the MR signal at the fully relaxed condition – the M0, using the single-compartment model (Alsop et al., 2014). Over the past decades, a variety of ASL techniques have been proposed, which can be roughly divided into four classes: pulsed ASL, continuous ASL (CASL), pseudo-CASL (PCASL), and velocity-selective ASL (VS-ASL) (Luis Hernandez-Garcia, 2022; Qin Qin, 2022). PASL uses a short-duration RF pulse to invert magnetization of arterial blood water, while CASL or PCASL uses a train of RF pulses with small flip angles to continuously drive the arterial blood water magnetization from the positive to the negative direction (Dai et al., 2008). PCASL represents the current state-of-art ASL technique. VS-ASL can theoretically avoid the post-labeling delay time and may become a future standard in ASL (Qin et al., 2022) but thus far VS-ASL has not been rarely used in AD research. Both PASL and PCASL have been implemented as commercial products by major MR vendors and are widely available in the clinical MR machine.

Since the inception of ASL MRI, it has been applied to a large body of translational research including aging and AD studies (John A Detre et al., 2012; Detre et al., 2009; Haller et al., 2016; Telischak et al., 2015). ASL MRI is particularly appealing to aging and AD research

because it is non-invasive and non-radioactive and can be repeated many times (Wang, 2014; Wolk & Detre, 2012). More importantly, the regional CBF maps measured by ASL MRI can be used a marker of regional brain function and its alterations by disease pathology. In fact, low CBF may even represent a major cause of AD pathology and subsequent cognitive decline(Zlokovic, 2005). Over the past decades, ASL MRI has been increasingly studied in the AD continuum, and the most consistent CBF change pattern in AD is the hypoperfusion in the temporoparietal cortex, which correlates with disease severity (Hu et al., 2010; Wang, 2014; Ze Wang, 2013) In addition to these cross-sectional findings, two recent studies have reported the longitudinal CBF reductions in AD and patients with mild cognitive impairment (MCI) (Camargo et al., 2021; Duan et al., 2021).

While the findings shown in current ASL MRI-based AD research literature are highly encouraging, a challenge is that AD ASL MRI data have been acquired with different ASL MRI sequences, especially in some multi-site longitudinal studies such as the Alzheimer's Disease Neuroimaging Initiative (ADNI)(http://adni.loni.usc.edu/). It is unknown how these acquisition variabilities (sequences and scanner vendors) affect the CBF alteration detections in the AD continuum. Thus far, only one paper has been published assessing the effects of three ASL MRI sequences on CBF difference detection between MCI and normal elderly control (NC) (Dolui et al., 2017). The data were acquired in Siemens MR machine with a 2D PASL, a 2D PCASL (without background suppression (BS)) and a 3D PCASL (with BS) sequence developed at the University of Pennsylvania (Vidorreta et al., 2014; Vidorreta et al., 2017; Vidorreta et al., 2012; Wu et al., 2007). This paper differed from the previous study by comparing three product ASL MRI sequences from two major MR vendors for assessing CBF difference between NC and MCI and AD. The sequences included the 2D Gradient Echo-Planar Imaging-based PASL MRI sequence from Siemens Healthineers (abbreviated as 2D PASL), the 3D Turbo Gradient Spin Echo-based PASL MRI sequence from Siemens Healthineers (3D PASL), and the 3D Fast Spin Echo-based PCASL MRI sequence from GE Healthcare (3D PCASL). The MR vendors included Siemens and GE. 2D PASL and 3D PASL are both based on Cartesian readout but the former is without BS and the latter is with BS; 3D PCASL is based on a stack of spiral readout and BS (Dai et al., 2008). Our first aim was to compare the sequences for differentiating patients with MCI from NC and patients with AD from MCI, and AD from NC. The second aim was to examine whether CBF calculated from the different ASL MRI data shows different sensitivity to the potential associations between regional CBF in NC, MCI, and AD subjects and memory as measured by the immediate recall total score (LIMM) (Chelune et al., 1990). We focused on memory because memory loss is a hallmark symptom of AD(Jahn, 2013) and LIMM is a typical measure of memory function with lower LIMM scores corresponding to severer memory decline. Previous studies have shown a positive correlation between CBF (measured by ASL MRI) LIMM (Leeuwis et al., 2017; Leeuwis et al., 2018). Comparing the CBF versus memory correlations revealed by different ASL sequences can provide additional information for evaluating the sequences for AD research.

MATERIALS AND METHODS

Subject Information

All data included in this study were from the ADNI including both the phase 2 and 3 (ADNI 2, ADNI 3). Subjects were separated into three groups NC, MCI, and AD according to their diagnostic status at the time the ASL MRI images were acquired. The 2D PASL data contained 25 NC, 25 MCI, and 25 AD subjects; the 3D PCASL data had 40 NC, 25 MCI, and 16 AD subjects; the 3D PASL data contained 35 NC, 25 MCI, and 16 AD. ADNI initially was launched in 2003 by the National Institute on Aging (NIA), the National Institute of Biomedical Imaging and Bioengineering (NIBIB), the US Food and Drug Administration, private pharmaceutical companies, and non-profit organizations, as a 60 million, five-year public-private partnership. Michael W. Weiner, MD, from San Francisco Veterans Affairs Medical Center and the University of California-San Francisco, is the principal investigator of ADNI. For this study, the inclusion criteria were that all the subjects must have ASL MRI (2D or 3D) and the structural MPRAGE images. Age, sex, years of education, LIMM were extracted from the files PTDEMOG.csv, and NEUROBAT.csv, respectively. The scores were matched according to the ASL MRI data acquisition dates. Note that the 2D PASL data had more MCI patients than the other two data types, we randomly selected 25 to be included in this study to match the number of MCI patients in the other two ASL datasets. Tables 1, 2, and 3 show the demographic and clinical information for 2D PASL, 3D PCASL, and 3D PASL.

Image Acquisitions

Detailed imaging data acquisition protocols can be found in http://adni.loni.usc.edu/methods/mri-tool/mri-acquisition/. All ASL MRI data were acquired with 3T MR scanners. The acquisition parameters are listed in Table 4 and described below:

2D PASL (from ADNI 2): The structural MR images were acquired using a T1-weighted 3D magnetization-prepared rapid gradient echo (MPRAGE) sequence with the following parameters: repetition time (TR)/echo time (TE)/inversion time (TI) = 2300/2.98/900 ms, 176 sagittal slices, within plane field-of-view (FOV) = 256 × 240 mm^2, voxel size = 1.1 × 1.1 × 1.2 mm^3, flip angle = 9°, bandwidth = 240 Hz/pixel. ASL data were acquired with the Siemens product 2D PASL sequence using the following parameters: TR/TE = 3400/12 ms, TI1/TI2 = 700/1900 ms, FOV = 256 mm, 24 sequential 4 mm thick slices with a 25% gap between the adjacent slices, partial Fourier factor = 6/8, bandwidth = 2368 Hz/pix, imaging matrix = 64 × 64, 50 pairs of label and control images. A M0 image is acquired in the beginning of the ASL scan using the shortest TE and long TR. This image is to measure the baseline magnetization (at the equilibrium state) of tissue signal to be used for perfusion signal calibration during CBF calculation.

3D PCASL and 3D PASL from ADNI 3: structural MRIs were acquired using the 3D MPRAGE sequence with the following parameters: TR/TE/TI = 2300/2.98/900 ms, voxel size = 1×1×1 mm^3, FOV = 208×240×256 mm^3. ASL images were acquired with the following parameters: TR/TE = 4885/10.5 ms, PLD = 2000 ms, voxel size = 1.9×1.9×4 mm^3, FOV = 240×240×160 mm^3. The 3D PASL data did not contain M0 scans but the

3D PCASL data did. Further information of the image acquisition can be found in http://adni.loni.usc.edu/data-samples/mri.

Absolute CBF value can be calculated from both the 2D PASL data and the 3D PCASL data but not the 3D PASL data because of the lack of M0 images in the 3D PASL data. To allow comparisons among the three types of ASL data, we calculated relative CBF for all three datasets.

2D PASL data processing

Similar to our previous studies (Camargo et al., 2021; Ze Wang, 2013), ASLtbx (Wang et al., 2008) was used for preprocessing all MR images. The processing steps included motion correction (Wang, 2012), temporal denoising through a high pass filtering and temporal nuisance regression, spatial smoothing, CBF quantification, outlier cleaning (Li et al., 2018), partial volume correction, and spatial registration to the Montreal Neurology Institute (MNI) standard brain space. Temporal nuisances including head motion time courses (3 translations and 3 rotations), and the cerebrospinal fluid (CSF) mean signal time course were regressed out from ASL image series at each voxel. CSF mask was defined during the structural MR image segmentations (see below). Spatial smoothing was performed with an isotropic Gaussian kernel with a full-width-at-half-maximum of 6 mm. The preprocessed ASL label and control image pairs were successively subtracted. The difference was subsequently converted into a quantitative CBF map using the one-compartment model included in ASLtbx.

Structural images were segmented into grey matter (GM), white matter (WM), and CSF using the segmentation tool provided in SPM12. The GM/WM/CSF images were projected into the native ASL image space based on the spatial transform obtained from the mean ASL control image versus structural MRI registration. The GM/WM/CSF probability was used to correct partial volume effect (PVE) at each GM voxel using a previously described approach (Du et al., 2006). The PVE corrected CBF map was then registered into the structural image space using the same mean ASL control image versus structural MRI registration transform. We calculated rCBF maps by dividing the absolute CBF at each voxel by the whole brain mean CBF value (mean CBF of the GM and WM. GM and WM masks were created during structural MRI segmentation and registration (see above)). For the CBF or rCBF versus LIMM correlation analysis, we only focused on regions defined by the meta-region-of-interest (meta-ROI) (Landau et al., 2012) which consists seven spheric ROIs in the left and right hippocampus, left and right angular gyrus, and left and right temporal lobe, and precuneus. CBF and rCBF were extracted from the five ROIs: the composite meta-ROI, the bilateral hippocampus, bilateral angular gyrus, bilateral temporal lobes, and precuneus. Correlation between LIMM and mean rCBF of each ROI was assessed separately using simple regression. Age and sex were included as covariates. These correlation analyses were performed for NC, MCI, and AD separately for each type of ASL CBF images.

3D PASL and 3D PCASL Data Processing

The processing steps for 3D ASL data were very similar to the 2D ASL processing with a few changes depending on the labeling approach. For 3D PASL data, rCBF was

computed at each voxel by dividing the perfusion signal by the whole brain mean (mean value of the GM and WM). For 3D PCASL, rCBF images was calculated by dividing the absolute CBF map by the whole brain mean (mean CBF of the GM and WM. GM and WM masks were obtained through structural MRI based brain segmentations). Structural MRI segmentations for both 3D PCASL and 3D PASL were performed using FreeSurfer (surfer.nmr.mgh.harvard.edu/). The corresponding GM/WM/CSF masks were registered native ASL MRI space to be used for calculating rCBF and for extracting the temporal nuisances for data preprocessing. CBF and rCBF were extracted from the five ROIs and correlated to LIMM using the approach described in previous section.

Statistical Analysis

One-way analysis of variance (ANOVA) was used to assess the group differences for continuous variables and X^2 for the categorical variables (sex). The results were presented in the form of mean ± standard deviation. Partial correlation was used to assess the correlations between regional CBF and LIMM, age sex, and years of education were used as nuisance variables and the results were corrected for multiple comparisons using Bonferroni correction. These neurobehavior scores were assessed on dates closest to that of the ASL-MRI scans.

Site effects were controlled with ComBat (Fortin et al., 2017). Two-sample t-test as implemented in SPM12 was used to assess the voxel-wise CBF difference between NC and MCI, MCI and AD, and NC and AD. Sex, age, and education years were included as covariates. The same voxelwise statistical analyses were performed for both the absolute CBF and rCBF separately. A voxel-wise statistical significance threshold was set to p-value < 0.001. The Monte Carlo simulation-based cluster size estimation was used for correcting the multiple comparisons. The cluster size threshold was found to be <=200, then used to threshold the suprathreshold clusters for all the analysis. BSPVIEW (bobspunt.com/software/bspmview) was used to visualize the image wise statistical analysis results.

RESULTS

Subject Information

Significant differences of MMSE and LIMM were found between NC, MCI, and AD subjects in the three cases: 2D PASL, 3D PCASL, and 3D PASL. In aging and AD, MMSE and LIMM inversely indicate the cognitive deficits and lower scores indicate severer cognitive decline or impairment. For the cohort included in this study, both MMSE and LIMM decrease with disease severity in the direction of NC>MCI>AD (see tables 1, 2, and 3). Based on 2D PASL, mean GM CBF in the NC/MCI/AD were: 26.61/19.55/18.13 ml/100g/min. Mean GM CBF was not significantly different between NC and MCI (p=0.086), but was significantly different between MCI and AD (p=1.00e-6) and between NC and AD (p=1.14e-7). For 3D PCASL data, the mean GM CBF of NC/MCI/AD was 29.59/27.51/26.77 ml/100g/min, respectively. Mean GM CBF did not significantly differ between NC and MCI (p=0.9487), but significantly differed between MCI and AD (p=3.40e-6) and between NC and AD (p=5.13e-5).

Voxel-wise CBF/rCBF Comparison between NC and MCI subjects

Fig 1 shows the results of the voxel-wise CBF comparisons (two-sample t-test) between NC and MCI subjects for 2D PASL, 3D PCASL, and 3D PASL. Fig 2 shows the voxel-wise NC versus MCI CBF comparison results for 2D PASL and 3D PCASL. Regardless of CBF and rCBF, 3D PCASL showed the highest sensitivity in terms of the group level CBF difference cluster size and peak t-values in the fronto-parietal regions. Using 2D PASL, MCI showed statistically significantly lower rCBF compared with NC subjects in the right superior orbital gyrus, right rectal gyrus, and right inferior temporal gyrus. For 3D PCASL, MCI patients showed significantly lower rCBF compared to NC subjects in the right middle frontal gyrus; and a significantly higher rCBF in MCI compared to NC subjects in the right superior medial gyrus, left precuneus, and right thalamus. For 3D PASL, significantly lower rCBF in MCI as compared to NC was found in the left and right temporal gyrus, right middle temporal gyrus, right amygdala, and left caudate nucleus; significantly higher rCBF in MCI compared with NC were found in the left superior parietal lobule, right superior frontal gyrus, right precuneus, and right cerebellum.

Voxel-wise CBF/rCBF Comparison between MCI and AD

Fig 3 shows the voxel-wise MCI versus AD rCBF comparison (two-sampled t-test) results for 2D PASL, 3D PCASL, and 3D PASL. Compared to the 2D PASL sequence, the 3D sequences showed higher sensitivity for the MCI minus AD rCBF difference detection. For 2D PASL, compared to MCI, AD showed significantly higher rCBF in the medial orbito-frontal cortex, lateral orbitofrontal cortex, and caudate, but lower rCBF in the cerebellum. For 3D PCASL, compared to MCI, AD had significantly higher rCBF in medial orbitofrontal cortex, lateral orbito-frontal cortex, striatum, temporal pole, middle temporal cortex including hippocampus, insula, and superior temporal cortex, dorsal anterior cingulate cortex, and cerebellum, but showed significantly lower rCBF the superior part of the prefrontal cortex, the superior part of the caudate, posterior cingulate cortex, and parietal cortex. For 3D PASL, significantly higher rCBF in AD compared to MCI was found in the orbito-frontal cortex, insula, striatum, temporal cortex, anterior cingulate cortex, fusiform, visual cortex, and cerebellum. Fig 4 shows the voxel-wise MCI-AD absolute CBF comparison results for the 2D PASL and 3D PCASL data. For both types of data, the MCI-AD absolute CBF difference patterns (Fig. 4A for 2D PASL, Fig. 4B for 3D PCASL) were quite similar to those identified by the corresponding rCBF (Fig. 3A and 3B for 2D PASL and 3D PCASL, respectively).

Voxel-wise CBF/rCBF Comparisons between NC and AD

Fig 5 shows results of the voxel-wise NC versus AD rCBF comparisons (two-sample t-test). 3D sequences showed higher sensitivity than 2D. 2D PASL did not show any significant rCBF difference between NC and AD. Using 3D PCASL, AD had significantly lower rCBF in left and right inferior and superior parietal lobule, left and right middle occipital gyrus but higher rCBF in the left and right cerebellum, left and right superior orbital gyrus, left and right hippocampus, left amygdala, and left putamen. Based on 3D PASL, AD showed significantly lower rCBF in the right thalamus, left and right caudate nucleus, left putamen, left superior frontal gyrus, and left and right precentral gyrus, but higher rCBF in the left

and right rectal gyrus, left and right temporal lobe, and left orbito-frontal gyrus. Fig 6 shows the voxel-wise NC-AD absolute CBF comparison results for the 2D PASL and 3D PCASL. 2D PASL revealed significantly lower CBF in AD compared to NC in the left precuneus. 3D PCASL showed significantly CBF reductions in AD compared to NC in the left and right cerebellum, left putamen, left insula lobe, left and right temporal lobe, and left and right superior orbital gyrus.

Correlations between regional CBF and LIMM Scores

This section lists the CBF or rCBF versus episodic memory (measured by LIMM) correlation analysis results. CBF or rCBF were extracted from the five ROIs. Regression analyses were performed for each type of data from each of the three populations: NC, MCI, and AD, separately. Each of the five ROIs was analyzed separately. Age, sex, and education years were covariated out. Absolute CBF did not show significant correlation to LIMM. For rCBF, 2D PASL and 3D PCASL showed significant (after multiple comparison correction) correlations. Positive rCBF versus LIMM correlations were found in 2D PASL in angular gyrus ($r = 0.51$, p-value = 0.003, 95% confidence interval: [0.33 0.66]) and the composite meta-ROI ($r = 0.45$, p-value = 0.009, 95% confidence interval: [0.26 0.61]). Negative rCBF versus LIMM correlations were found in 3D PCASL in angular gyrus ($r = -0.74$, p-value = 0.004, 95% confidence interval: [−0.83 −0.62]), the composite meta-ROI ($r=-0.73$, $p=0.005$, 95% confidence interval: [−0.82 −0.61]), and hippocampus ($r = -0.844$, p-value = 0.0003, 95% confidence interval: [−0.9 −0.77]). See supplementary information for the scatter plots.

DISCUSSION

Using existing data from ADNI, we compared three commercial ASL MRI sequences: 2D PASL, 3D PCASL, and 3D PASL for the efficacy of detecting the CBF and rCBF differences between NC and patients with MCI or AD and between MCI and AD. Our results showed that 3D PCASL showed the highest sensitivity for the between-group CBF or rCBF differences than the other two ASL sequences; 2D PASL showed the lowest sensitivity for detecting those differences. It did not even show any statistically significant CBF or rCBF difference between NC and AD. For neurocognitive correlation analyses, 2D PASL showed positive rCBF versus memory correlations in angular gyrus and the composite meta-ROI; while 3D PCASL revealed negative correlations between memory and rCBF in angular gyrus, the composite meta-ROI, and hippocampus. The novel contributions and findings of this work included that: we assessed cross-sectional CBF and rCBF difference among three types of cohorts: NC, MCI, and AD using three types of ASL MRI in a single study; the cross-sectional CBF/rCBF difference identified by 3D PCASL are spatially more distributed than those reported in the literature; compared to NC, we found mainly lower absolute CBF in MCI but both higher and lower CBF in AD; the rCBF based group comparisons showed lower frontal rCBF and higher parietal rCBF using the 3D PCASL and 3D PASL sequences; absolute CBF in orbitofrontal cortex appeared to be consistently affected by disease status change: it first reduced in MCI compared to NC and then increased in AD as compared to MCI.

The sensitivity differences between the three commercial ASL MRI sequences are consistent with the ASL technique development and evaluation literature (Fernandez-Seara et al., 2005; Gunther et al., 2005; Mutsaerts et al., 2014; Mutsaerts et al., 2015; Nanjappa et al., 2021; Steketee et al., 2015; Vidorreta et al., 2012). Higher sensitivity of the 3D sequences may be contributed by BS, which significantly increases the signal-to-noise-ratio (SNR) of the ASL MRI signal by nulling the strong background tissue signal. The relatively higher sensitivity of PCASL compared to PASL may be contributed by the stronger signal from the labeled arterial blood during the longer arterial spin labeling duration in PCASL compared to PASL. It may also be contributed by the better background signal control in PCASL (Alsop et al., 2014; Jezzard et al., 2018; Luis Hernandez-Garcia, 2022).

The cross-sectional comparison results were consistent with the AD/MCI ASL imaging research literature. For both 3D PASL and 3D PCASL, a common lower CBF and rCBF pattern in MCI in relative to NC was found in the left and right middle orbital gyrus and left and right temporal lobe. Temporal lobe is pivotal in memory and is associated with auditory information processing, language, emotion, and part of visual perception. Temporal lobe CBF reductions in both MCI and AD have been observed using ASL MRI in several studies (Alsop et al., 2010; Dai et al., 2009; Wolk & Detre, 2012). Hypoperfusion in MCI as compared to NC was found in the left and right precuneus, left and right angular gyrus, and left and right cerebellum. Hypoperfusion in precuneus was consistent with previous findings reported by other groups and us (Binnewijzend et al., 2013; Camargo et al., 2021; Chao et al., 2009). Hypoperfusion in cerebellum was consistent with our recent ADNI data based longitudinal CBF study (Camargo et al., 2021), and may reflect a decline of cerebellum functions in MCI (Jacobs et al., 2018). 3D PCASL revealed a statistically significant global CBF reduction in MCI patients in relative to NC, which is supported by our previous work (Ze Wang, 2013) and by the CBF reduction trend in MCI compared to NC reported in (Lövblad et al., 2015). After controlling this global CBF change in the rCBF-based analyses, 3D PCASL revealed hyperperfusion (lower rCBF in MCI than NC) patterns in the limbic area, prefrontal cortex, temporal cortex, posterior cingulate cortex/precuneus while the hypoperfusion patterns in orbito-frontal cortex, temporal cortex, and temporal cortex remained. The presence of both rCBF-derived hypoperfusion and hyperperfusion indicates a redistribution of CBF in MCI, which might represent a mechanism for compensating the functional impairment caused by MCI. Our data did not show a global CBF difference between MCI and AD. Both 2D PASL and 3D PCASL showed higher CBF in medial orbito-frontal cortex in AD in relative to MCI. 3D PCASL showed spatially more distributed hypo-perfusion (higher in AD than MCI) and hyperperfusion (higher in MCI than AD). The rCBF-based MCI-AD differences in 2D PASL and 3D PCASL are quite similar to those found in the absolute CBF images. 3D PASL only showed hyperperfusion (higher rCBF in AD than MCI), which is not consistent with the aforementioned AD CBF literature. The NC-AD differences are approximately the summation of the NC-MCI and MCI-AD differences. 2D PASL did not find any statistically significant CBF/rCBF differences between NC and AD. This mis-detection suggests a low sensitivity of 2D PASL, which may be mainly caused by the low SNR. 3D PCASL revealed reduced CBF in most of the cortex except for the prefrontal part. Using rCBF, 3D PCASL and 3D PASL both showed hyper-perfusion (higher rCBF in AD than NC) in prefrontal cortex and the anterior and

lateral part of the limbic system but hypo-perfusion (lower rCBF in AD than NC) in the back of the brain. This bidirectional rCBF change pattern: frontal hyper-perfusion and posterior hypoperfusion in AD matched the findings in our previous study (Hu et al., 2010).

Interestingly, the seemingly least sensitive 2D PASL showed significant rCBF versus memory correlations. 3D PASL did not find any significant CBF/rCBF versus memory correlations. 3D PCASL showed negative rCBF versus memory correlations. Because the ROIs are defined from the regions with hypo-metabolism or hypo-perfusion in AD, the positive rCBF versus memory correlations in these regions identified by 2D PASL means that lower CBF (in relative to the whole brain mean) reflects the severity of clinical symptoms of the AD patients. The seemingly contradictory findings in 3D PCASL might be contributed by the relatively larger CBF variations (3D PCASL yielded higher CBF value than 2D PASL) and the smaller sample size. Regressing out age and sex may have disproportional effects on the CBF/rCBF versus memory associations. For example, we observed positive correlation between the meta-ROI and hippocampus ROI CBF and the LIMM score in 3D PCASL but not in the 2D PASL before regressing out age and sex. But we did not find any significant correlation after regressing out age and sex.

Several studies have compared different ASL sequences in healthy subjects using the same or different vendor machine (Mutsaerts et al., 2014; Mutsaerts et al., 2015; Nanjappa et al., 2021; Steketee et al., 2015; Vidorreta et al., 2012). The value of this study is the cross-sectional comparison of ASL MRI for normal aging, MCI, and AD, which are often very difficult to be recruited to a sequence comparison project using the within-subject design. Another new contribution is that the sequences are commercial products from two different vendors, while previous studies focused on laboratory-use ones.

We should note some limitations of this study. First, the sample size was modest. Particularly, there were fewer AD patients in the 3D PASL and 3D PCASL cohorts. The small sample size plus the multi-site data acquisition make it difficult to fully attribute the observed between-sequence discrepancy of the patient versus control or MCI versus AD CBF change patterns. Data harmonization through ComBat can not control other unknown factors such as environment or diet or life style, which can all contribute to CBF/rCBF changes. These factors may also be part of the reason for the contradictory rCBF versus memory associations found in 2D PASL and 3D PCASL. Second, 3D PASL data did not contain an M0 scan for calculating the absolute CBF value. This technical issue should be solved in future data acquisitions so the 3D PASL and 3D PCASL sequences can be directly compared based on the quantitative CBF. A third limitation is that all ASL data were acquired with a single post-labeling delay (PLD) time, which might be shorter than the real arterial transit time (time for the labeled arterial blood to transit from the labeling plane or labeling location to the imaging site). However, as the PLD used in ADNI (1.9 s for 2D PASL and 2s for 3D PASL and 3D PCASL) was longer than or similar to the arterial transit time (ATT) of NC, MCI, and AD reported in the literature (Liu et al., 2012; Sun et al., 2022; Tsujikawa et al., 2016), the possibility of having a shorter than expected PLD should be low for most of brain regions. For brain regions with an ATT>PLD, the observed group level CBF/rCBF difference may be partially contributed by the potential group level ATT difference. To fully delineate these two components, we will need to measure ATT using the

multi-PLD ASL MRI or the Hadmard encoded ASL (MacIntosh et al., 2010; Wells et al., 2010) or the slice timing based global ATT estimation method (Aldo Camargo, 2022).

CONCLUSION

In terms of group level CBF/rCBF changes among the different stages of the AD continuum, 3D PCASL (with BS) provides the highest sensitivity than 3D PASL (with BS) and 2D PASL. CBF in orbito-frontal cortex presents a U-shaped change pattern from normal aging to MCI and to AD. The value of 3D PCASL for assessing the neurocognitive correlates of CBF/rCBF needs more data to be fully evaluated.

Supplementary Material

Refer to Web version on PubMed Central for supplementary material.

ACKNOWLEDGEMENTS

Data collection and sharing for this project were funded by the Alzheimer's Disease Neuroimaging Initiative (ADNI) (National Institutes of Health Grant U01 AG024904) and DOD ADNI (Department of Defense award number W81XWH-12-2-0012). ADNI is funded by the National Institute on Aging, the National Institute of Biomedical Imaging and Bioengineering, and through generous contributions from the following: AbbVie, Alzheimer's Association; Alzheimer's Drug Discovery Foundation; Araclon Biotech; BioClinica, Inc.; Biogen; Bristol-Myers Squibb Company; CereSpir, Inc.; Cogstate; Eisai Inc.; Elan Pharmaceuticals, Inc.; Eli Lilly and Company; EuroImmun; F. Hoffmann-La Roche Ltd and its affiliated company Genentech, Inc.; Fujirebio; GE Healthcare; IXICO Ltd.; Janssen Alzheimer Immunotherapy Research & Development, LLC.; Johnson & Johnson Pharmaceutical Research & Development LLC.; Lumosity; Lundbeck; Merck & Co., Inc.; Meso Scale Diagnostics, LLC.; NeuroRx Research; Neurotrack Technologies; Novartis Pharmaceuticals Corporation; Pfizer Inc.; Piramal Imaging; Servier; Takeda Pharmaceutical Company; and Transition Therapeutics. The Canadian Institutes of Health Research is providing funds to support ADNI clinical sites in Canada. Private sector contributions are facilitated by the Foundation for the National Institutes of Health (www.fnih.org). The grantee organization is the Northern California Institute for Research and Education, and the study is coordinated by the Alzheimer's Therapeutic Research Institute at the University of Southern California. ADNI data are disseminated by the Laboratory for Neuroimaging at the University of Southern California.

FUNDING

This work was supported by NIH grants: R01AG060054, R01AG070227, R01EB031080-01A1, P41EB029460-01A1, 1UL1TR003098.

Availability of data and materials

ADNI data are freely available from https://adni.loni.usc.edu/. ASLtbx is freely available from https://cfn.upenn.edu/zewang/ASLtbx.php

REFERENCES

Aldo Camargo ZW (2022). Estimating Arterial Transit Time (ATT) From ASL MRI Acquired at A Single Post-Labeling-Delay Time 2022 Annual Meeting of the International Society of Magnetic Resonance in Medicine, London.

Alsop DC, Casement M, de Bazelaire C, Fong T, & Press DZ (2008, Oct 1). Hippocampal hyperperfusion in Alzheimer's disease. NeuroImage, 42(4), 1267–1274. [PubMed: 18602481]

Alsop DC, Dai W, Grossman M, & Detre JA (2010). Arterial spin labeling blood flow MRI: its role in the early characterization of Alzheimer's disease. Journal of Alzheimer's disease : JAD, 20(3), 871–880. 10.3233/JAD-2010-091699 [PubMed: 20413865]

Alsop DC, Detre JA, Golay X, Gunther M, Hendrikse J, Hernandez-Garcia L, Lu H, Macintosh BJ, Parkes LM, Smits M, van Osch MJ, Wang DJ, Wong EC, & Zaharchuk G (2014, Apr 8). Recommended implementation of arterial spin-labeled perfusion MRI for clinical applications: A consensus of the ISMRM perfusion study group and the European consortium for ASL in dementia. Magn Reson Med. 10.1002/mrm.25197

Alsop DC, Detre JA, & Grossman M (2000). Assessment of cerebral blood flow in Alzheimer's disease by spin-labeled magnetic resonance imaging. Annals of neurology, 47(1), 93–100. [PubMed: 10632106]

Baron JC, Lebrun-Grandie P, Collard P, Crouzel C, Mestelan G, & Bousser MG (1982, May). Noninvasive measurement of blood flow, oxygen consumption, and glucose utilization in the same brain regions in man by positron emission tomography: concise communication. Journal of nuclear medicine : official publication, Society of Nuclear Medicine, 23(5), 391–399. http://www.ncbi.nlm.nih.gov/pubmed/6978932 [PubMed: 6978932]

Binnewijzend MA, Kuijer JP, Benedictus MR, van der Flier WM, Wink AM, Wattjes MP, van Berckel BN, Scheltens P, & Barkhof F (2013, Apr). Cerebral blood flow measured with 3D pseudocontinuous arterial spin-labeling MR imaging in Alzheimer disease and mild cognitive impairment: a marker for disease severity. Radiology, 267(1), 221–230. 10.1148/radiol.12120928 [PubMed: 23238159]

Camargo A, Wang Z, & Alzheimer's Disease Neuroimaging I (2021). Longitudinal Cerebral Blood Flow Changes in Normal Aging and the Alzheimer's Disease Continuum Identified by Arterial Spin Labeling MRI. Journal of Alzheimer's disease : JAD, 81(4), 1727–1735. 10.3233/JAD-210116 [PubMed: 33967053]

Chao LL, Pa J, Duarte A, Schuff N, Weiner MW, Kramer JH, Miller BL, Freeman KM, & Johnson JK (2009, Jul-Sep). Patterns of cerebral hypoperfusion in amnestic and dysexecutive MCI. Alzheimer Dis Assoc Disord, 23(3), 245–252. 10.1097/WAD.0b013e318199ff46 [PubMed: 19812467]

Chelune GJ, Bornstein RA, & Prifitera A (1990). The Wechsler memory scale—revised. In Advances in psychological assessment (pp. 65–99). Springer.

Dai W, Garcia D, de Bazelaire C, & Alsop DC (2008, Dec). Continuous flow-driven inversion for arterial spin labeling using pulsed radio frequency and gradient fields. Magn Reson Med, 60(6), 1488–1497. 10.1002/mrm.21790 [PubMed: 19025913]

Dai W, Lopez OL, Carmichael OT, Becker JT, Kuller LH, & Gach HM (2009, Mar). Mild cognitive impairment and alzheimer disease: patterns of altered cerebral blood flow at MR imaging. Radiology, 250(3), 856–866. https://doi.org/2503080751 [pii] 10.1148/radiol.2503080751 [PubMed: 19164119]

Detre JA, Leigh JS, Williams DS, & Koretsky AP (1992). Perfusion imaging. Magnetic Resonance in Medicine, 23, 37–45. [PubMed: 1734182]

Detre JA, Rao H, Wang DJ, Chen YF, & Wang Z (2012, May). Applications of arterial spin labeled MRI in the brain [Research Support, N.I.H., Extramural]. Journal of magnetic resonance imaging : JMRI, 35(5), 1026–1037. 10.1002/jmri.23581 [PubMed: 22246782]

Detre JA, Rao H, Wang DJ, Chen YF, & Wang Z (2012). Applications of arterial spin labeled MRI in the brain. Journal of Magnetic Resonance Imaging, 35(5), 1026–1037. [PubMed: 22246782]

Detre JA, Wang J, Wang Z, & Rao H (2009, Aug). Arterial spin-labeled perfusion MRI in basic and clinical neuroscience. Current opinion in neurology, 22(4), 348–355. 10.1097/WCO.0b013e32832d9505 [PubMed: 19491678]

DeWitt DS, Yuan XQ, Becker DP, & Hayes RL (1988, Oct-Dec). Simultaneous, quantitative measurement of local blood flow and glucose utilization in tissue samples in normal and injured feline brain. Brain Inj, 2(4), 291–303. http://www.ncbi.nlm.nih.gov/pubmed/3203175 [PubMed: 3203175]

Dolui S, Vidorreta M, Wang Z, Nasrallah IM, Alavi A, Wolk DA, & Detre JA (2017, Jul 24). Comparison of PASL, PCASL, and background-suppressed 3D PCASL in mild cognitive impairment. Hum Brain Mapp. 10.1002/hbm.23732

Du AT, Jahng GH, Hayasaka S, Kramer JH, Rosen HJ, Gorno-Tempini ML, Rankin KP, Miller BL, Weiner MW, & Schuff N (2006, Oct 10). Hypoperfusion in frontotemporal dementia and Alzheimer disease by arterial spin labeling MRI. Neurology, 67(7), 1215–1220. 10.1212/01.wnl.0000238163.71349.78 [PubMed: 17030755]

Duan W, Zhou GD, Balachandrasekaran A, Bhumkar AB, Boraste PB, Becker JT, Kuller LH, Lopez OL, Gach HM, & Dai W (2021). Cerebral Blood Flow Predicts Conversion of Mild Cognitive Impairment into Alzheimer's Disease and Cognitive Decline: An Arterial Spin Labeling Follow-up Study. Journal of Alzheimer's disease, 82(1), 293–305.

Fernandez-Seara MA, Wang Z, Wang J, Rao HY, Guenther M, Feinberg DA, & Detre JA (2005, Nov). Continuous arterial spin labeling perfusion measurements using single shot 3D GRASE at 3 T. Magn Reson Med, 54(5), 1241–1247. 10.1002/mrm.20674 [PubMed: 16193469]

Fortin J-P, Parker D, Tunç B, Watanabe T, Elliott MA, Ruparel K, Roalf DR, Satterthwaite TD, Gur RC, & Gur RE (2017). Harmonization of multi-site diffusion tensor imaging data. Neuroimage, 161, 149–170. [PubMed: 28826946]

Furlow TW Jr., Martin RM, & Harrison LE (1983, Mar). Simultaneous measurement of local glucose utilization and blood flow in the rat brain: an autoradiographic method using two tracers labeled with carbon-14. J Cereb Blood Flow Metab, 3(1), 62–66. 10.1038/jcbfm.1983.7 [PubMed: 6822619]

Gunther M, Oshio K, & Feinberg DA (2005, Aug). Single-shot 3D imaging techniques improve arterial spin labeling perfusion measurements [Research Support, N.I.H., Extramural Research Support, U.S. Gov't, P.H.S.]. Magnetic resonance in medicine : official journal of the Society of Magnetic Resonance in Medicine / Society of Magnetic Resonance in Medicine, 54(2), 491–498. 10.1002/mrm.20580

Haller S, Zaharchuk G, Thomas DL, Lovblad K-O, Barkhof F, & Golay X (2016). Arterial spin labeling perfusion of the brain: emerging clinical applications. Radiology, 281(2), 337–356. [PubMed: 27755938]

Hu WT, Wang Z, Lee VM, Trojanowski JQ, Detre JA, & Grossman M (2010, Sep 7). Distinct cerebral perfusion patterns in FTLD and AD [Research Support, N.I.H., Extramural Research Support, Non-U.S. Gov't]. Neurology, 75(10), 881–888. 10.1212/WNL.0b013e3181f11e35 [PubMed: 20819999]

Jacobs HI, Hopkins DA, Mayrhofer HC, Bruner E, van Leeuwen FW, Raaijmakers W, & Schmahmann JD (2018). The cerebellum in Alzheimer's disease: evaluating its role in cognitive decline. Brain : a journal of neurology, 141(1), 37–47. [PubMed: 29053771]

Jahn H (2013, Dec). Memory loss in Alzheimer's disease. Dialogues Clin Neurosci, 15(4), 445–454. 10.31887/DCNS.2013.15.4/hjahn [PubMed: 24459411]

Jezzard P, Chappell MA, & Okell TW (2018, Jan 1). Arterial spin labeling for the measurement of cerebral perfusion and angiography. J Cereb Blood Flow Metab, 38(4), 603–626. 10.1177/0271678X17743240 [PubMed: 29168667]

Landau SM, Mintun MA, Joshi AD, Koeppe RA, Petersen RC, Aisen PS, Weiner MW, Jagust WJ, & Initiative A s. D. N. (2012). Amyloid deposition, hypometabolism, and longitudinal cognitive decline. Annals of neurology, 72(4), 578–586. [PubMed: 23109153]

Leeuwis AE, Benedictus MR, Kuijer JP, Binnewijzend MA, Hooghiemstra AM, Verfaillie SC, Koene T, Scheltens P, Barkhof F, & Prins ND (2017). Lower cerebral blood flow is associated with impairment in multiple cognitive domains in Alzheimer's disease. Alzheimers Dement (Amst), 13(5), 531–540.

Leeuwis AE, Smith LA, Melbourne A, Hughes AD, Richards M, Prins ND, Sokolska M, Atkinson D, Tillin T, & Jäger HR (2018). Cerebral blood flow and cognitive functioning in a community-based, multi-ethnic cohort: the SABRE study. Front Aging Neurosci, 10, 279. [PubMed: 30279656]

Li Y, Dolui S, Xie DF, Wang Z, & Alzheimer's Disease Neuroimaging I (2018, Sep 1). Priors-guided slice-wise adaptive outlier cleaning for arterial spin labeling perfusion MRI. J Neurosci Methods, 307, 248–253. 10.1016/j.jneumeth.2018.06.007 [PubMed: 29908993]

Liu Y, Zhu X, Feinberg D, Guenther M, Gregori J, Weiner MW, & Schuff N (2012). Arterial spin labeling MRI study of age and gender effects on brain perfusion hemodynamics. Magnetic Resonance in Medicine, 68(3), 912–922. [PubMed: 22139957]

Liu ZM, Schmidt KF, Sicard KM, & Duong TQ (2004, Aug). Imaging oxygen consumption in forepaw somatosensory stimulation in rats under isoflurane anesthesia. Magn Reson Med, 52(2), 277–285. 10.1002/mrm.20148 [PubMed: 15282809]

Lövblad K-O, Montandon M-L, Viallon M, Rodriguez C, Toma S, Golay X, Giannakopoulos P, & Haller S (2015). Arterial spin-labeling parameters influence signal variability and estimated regional relative cerebral blood flow in normal aging and mild cognitive impairment: fAIR versus PICORE techniques. American Journal of Neuroradiology, 36(7), 1231–1236. [PubMed: 25882291]

Luis Hernandez-Garcia VA, Dai Weiying, Maria A Fernandez-Seara Jia Guo, Guenther Matthias, Schollenberger Jonas, Madhuranthakam Ananth J., Mutsaerts Henk, Petr Jan, Qin Qin, Suzuki Yuriko, Taso Manuel, Thomas David L., Matthias J P van Osch, Woods Joseph G, Zhao Moss Y, Yan Lirong, Wang Ze, Zhao Li, Okell Thomas W, ISMRM Perfusion Study Group. (2022). Recent technical developments in ASL: A Review of the State of the Art. Magn Reson Med. 10.1002/mrm.29381

MacIntosh BJ, Filippini N, Chappell MA, Woolrich MW, Mackay CE, & Jezzard P (2010). Assessment of arterial arrival times derived from multiple inversion time pulsed arterial spin labeling MRI. Magnetic Resonance in Medicine, 63(3), 641–647. [PubMed: 20146233]

Musiek ES, Chen Y, Korczykowski M, Saboury B, Martinez PM, Reddin JS, Alavi A, Kimberg DY, Wolk DA, Julin P, Newberg AB, Arnold SE, & Detre JA (2012, Jan). Direct comparison of fluorodeoxyglucose positron emission tomography and arterial spin labeling magnetic resonance imaging in Alzheimer's disease. Alzheimer's & dementia : the journal of the Alzheimer's Association, 8(1), 51–59. 10.1016/j.jalz.2011.06.003

Mutsaerts HJ, Steketee RM, Heijtel DF, Kuijer JP, van Osch MJ, Majoie CB, Smits M, & Nederveen AJ (2014). Inter-vendor reproducibility of pseudo-continuous arterial spin labeling at 3 Tesla. PLoS One, 9(8), e104108. [PubMed: 25090654]

Mutsaerts HJ, van Osch MJ, Zelaya FO, Wang DJ, Nordhoy W, Wang Y, Wastling S, Fernandez-Seara MA, Petersen ET, Pizzini FB, Fallatah S, Hendrikse J, Geier O, Gunther M, Golay X, Nederveen AJ, Bjornerud A, & Groote IR (2015, Jun). Multi-vendor reliability of arterial spin labeling perfusion MRI using a near-identical sequence: implications for multi-center studies. NeuroImage, 113, 143–152. 10.1016/j.neuroimage.2015.03.043 [PubMed: 25818685]

Nanjappa M, Troalen T, Pfeuffer J, Maréchal B, Hilbert T, Kober T, Schneider FC, Croisille P, & Viallon M (2021). Comparison of 2D simultaneous multi-slice and 3D GRASE readout schemes for pseudo-continuous arterial spin labeling of cerebral perfusion at 3 T. Magnetic Resonance Materials in Physics, Biology and Medicine, 34(3), 437–450.

Qin Q, Alsop DC, Bolar DS, Hernandez-Garcia L, Meakin J, Liu D, Nayak KS, Schmid S, van Osch MJ, & Wong EC (2022). Velocity-selective arterial spin labeling perfusion MRI: A review of the state of the art and recommendations for clinical implementation. Magnetic Resonance in Medicine, 88(4), 1528–1547. [PubMed: 35819184]

Qin Qin DCA, Bolar Divya S, Hernandez-Garcia Luis, Meakin James, Liu Dapeng, Nayak Krishna S, Schmid Sophie, Matthias J P van Osch, Wong Eric C, Woods Joseph G, Zaharchuk Greg, Zhao Moss Y, Zungho, Guo Jia, ISMRM Perfusion Study Group. (2022). Velocity-selective arterial spin labeling perfusion MRI: A review of the state of the art and recommendations for clinical implementation. Magn Reson Med. 10.1002/mrm.29371

Raichle ME (1998, Feb 3). Behind the scenes of functional brain imaging: a historical and physiological perspective. Proc Natl Acad Sci U S A, 95(3), 765–772. http://www.ncbi.nlm.nih.gov/entrez/query.fcgi?cmd=Retrieve&db=PubMed&dopt=Citation&list_uids=9448239 [PubMed: 9448239]

Solis E Jr, Hascup KN, & Hascup ER (2020). Alzheimer's disease: the link between amyloid-β and neurovascular dysfunction. Journal of Alzheimer's disease, 76(4), 1179–1198.

Steketee RM, Mutsaerts HJ, Bron EE, Van Osch MJ, Majoie CB, Van Der Lugt A, Nederveen AJ, & Smits M (2015). Quantitative functional arterial spin labeling (fASL) MRI–sensitivity and reproducibility of regional CBF changes using pseudo-continuous ASL product sequences. PLoS One, 10(7), e0132929. [PubMed: 26172381]

Sun M, Wang Y-L, Li R, Jiang J, Zhang Y, Li W, Zhang Y, Jia Z, Chappell M, & Xu J (2022). Potential Diagnostic Applications of Multi-Delay Arterial Spin Labeling in Early Alzheimer's Disease: The Chinese Imaging, Biomarkers, and Lifestyle Study. Frontiers in Neuroscience, 16.

Telischak NA, Detre JA, & Zaharchuk G (2015, May). Arterial spin labeling MRI: clinical applications in the brain. J Magn Reson Imaging, 41(5), 1165–1180. 10.1002/jmri.24751 [PubMed: 25236477]

Tsujikawa T, Kimura H, Matsuda T, Fujiwara Y, Isozaki M, Kikuta K. i., & Okazawa H (2016). Arterial transit time mapping obtained by pulsed continuous 3D ASL imaging with multiple post-label delay acquisitions: comparative study with PET-CBF in patients with chronic occlusive cerebrovascular disease. PLoS One, 11(6), e0156005. [PubMed: 27275779]

Vestergaard MB, Lindberg U, Aachmann-Andersen NJ, Lisbjerg K, Christensen SJ, Law I, Rasmussen P, Olsen NV, & Larsson HB (2016, Jun). Acute hypoxia increases the cerebral metabolic rate - a magnetic resonance imaging study. J Cereb Blood Flow Metab, 36(6), 1046–1058. 10.1177/0271678X15606460 [PubMed: 26661163]

Vidorreta M, Balteau E, Wang Z, De Vita E, Pastor MA, Thomas DL, Detre JA, & Fernandez-Seara MA (2014, Nov). Evaluation of segmented 3D acquisition schemes for whole-brain high-resolution arterial spin labeling at 3 T. NMR Biomed, 27(11), 1387–1396. 10.1002/nbm.3201 [PubMed: 25263944]

Vidorreta M, Wang Z, Chang YV, Wolk DA, Fernandez-Seara MA, & Detre JA (2017). Whole-brain background-suppressed pCASL MRI with 1D-accelerated 3D RARE Stack-Of-Spirals readout. PLoS One, 12(8), e0183762. 10.1371/journal.pone.0183762 [PubMed: 28837640]

Vidorreta M, Wang Z, Rodriguez I, Pastor MA, Detre JA, & Fernandez-Seara MA (2012, Nov 7). Comparison of 2D and 3D single-shot ASL perfusion fMRI sequences. NeuroImage, 66C, 662–671. 10.1016/j.neuroimage.2012.10.087

Wang Z (2012). Improving Cerebral Blood Flow Quantification for Arterial Spin Labeled Perfusion MRI by Removing Residual Motion Artifacts and Global Signal Fluctuations. Magnetic Resonance Imaging, 30(10), 1409–1415. 10.1016/j.mri.2012.05.004 [PubMed: 22789842]

Wang Z (2014). Characterizing Early Alzheimer's Disease and Disease Progression Using Hippocampal Volume and Arterial Spin Labeling Perfusion MRI. Journal of Alzheimers Disease, 42, S495–S502. https://doi.org/Doi 10.3233/Jad-141419

Wang Z (2022). Arterial Spin Labeling Perfusion MRI Signal Processing Through Traditional Methods and Machine Learning. Investigative Magnetic Resoance Imaging.

Wang Z, Aguirre GK, Rao H, Wang J, Fernández-Seara MA, Childress AR, & Detre JA (2008). Empirical optimization of ASL data analysis using an ASL data processing toolbox: ASLtbx. Magnetic Resonance Imaging, 26(2), 261–269. [PubMed: 17826940]

Wells JA, Lythgoe MF, Gadian DG, Ordidge RJ, & Thomas DL (2010, Apr). In vivo Hadamard encoded continuous arterial spin labeling (H-CASL). Magn Reson Med, 63(4), 1111–1118. 10.1002/mrm.22266 [PubMed: 20373414]

Wolk DA, & Detre JA (2012, Aug). Arterial spin labeling MRI: an emerging biomarker for Alzheimer's disease and other neurodegenerative conditions [Research Support, N.I.H., Extramural]. Current opinion in neurology, 25(4), 421–428. 10.1097/WCO.0b013e328354ff0a [PubMed: 22610458]

Wu WC, Fernandez-Seara M, Detre JA, Wehrli FW, & Wang J (2007, Nov). A theoretical and experimental investigation of the tagging efficiency of pseudocontinuous arterial spin labeling. Magn Reson Med, 58(5), 1020–1027. 10.1002/mrm.21403 [PubMed: 17969096]

Xu G, Rowley HA, Wu G, Alsop DC, Shankaranarayanan A, Dowling M, Christian BT, Oakes TR, & Johnson SC (2010, Apr). Reliability and precision of pseudo-continuous arterial spin labeling perfusion MRI on 3.0 T and comparison with 15O-water PET in elderly subjects at risk for Alzheimer's disease. NMR Biomed, 23(3), 286–293. 10.1002/nbm.1462 [PubMed: 19953503]

Ze Wang SRD, Sharon X. Xie, Arnold Steven E., Detre John A., Wolk David A., for the Alzheimer's Disease Neuroimaging Initiative. (2013). Arterial Spin Labeled MRI in Prodromal Alzheimer's Disease: A Multi-Site Study. Neuroimage: clinical, 2, 630–636. [PubMed: 24179814]

Zlokovic BV (2005, Apr). Neurovascular mechanisms of Alzheimer's neurodegeneration. Trends Neurosci, 28(4), 202–208. 10.1016/j.tins.2005.02.001 [PubMed: 15808355]

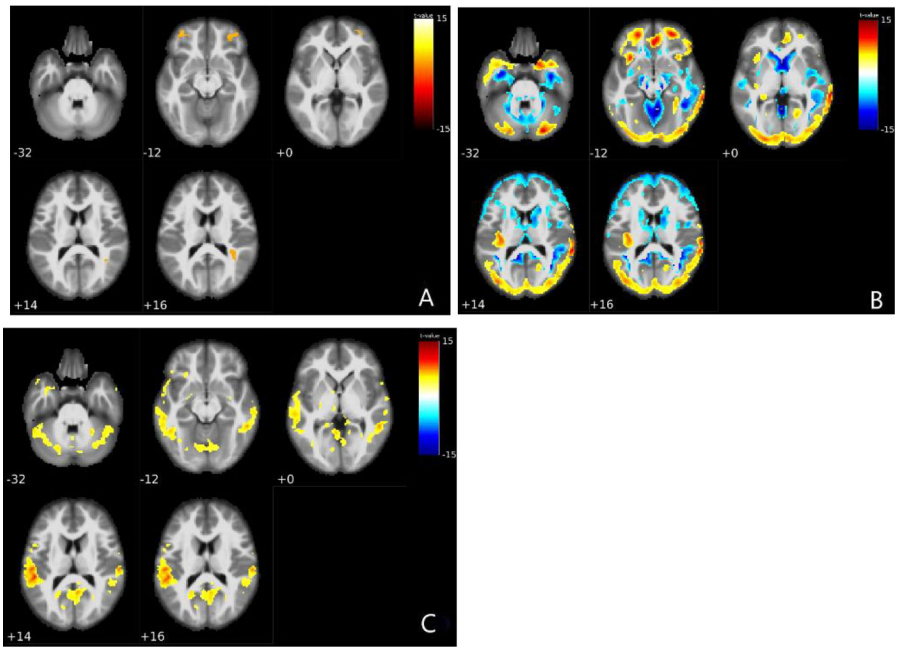

Figure 1:

rCBF difference between NC and MCI identified by three types of ASL data. A) 2D PASL, B) 3D PCASL, C) 3D PASL. Hot color means higher rCBF in NC; blue color means lower in NC. The color bar represents statistical significance (t) values. The number underneath each image slice indicate the slice location in the MNI standard brain space.

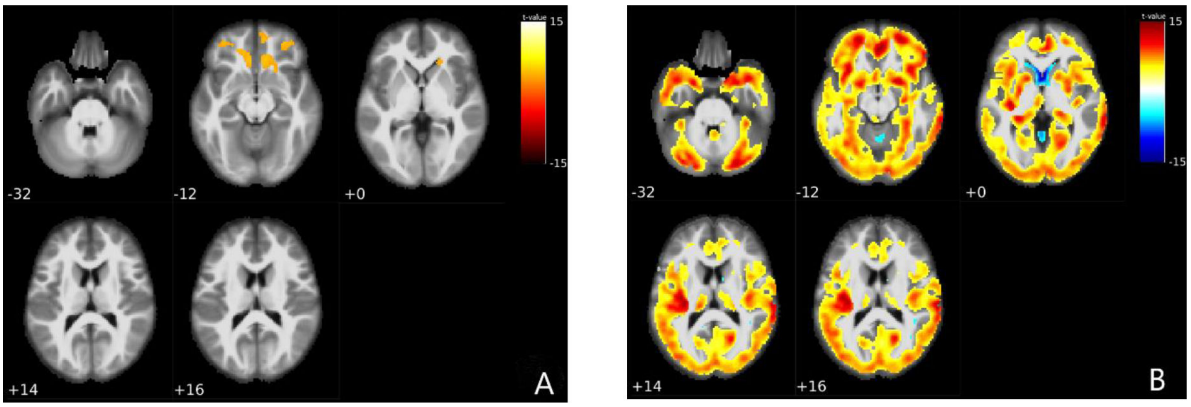

Figure 2:

CBF difference between NC and MCI identified by two types of ASL data. A) 2D PASL, and B) 3D PCASL. Hot color means higher CBF in NC; blue color means lower in NC. The color bar represents statistical significance (t) values. The number underneath each image slice indicate the slice location in the MNI standard brain space.

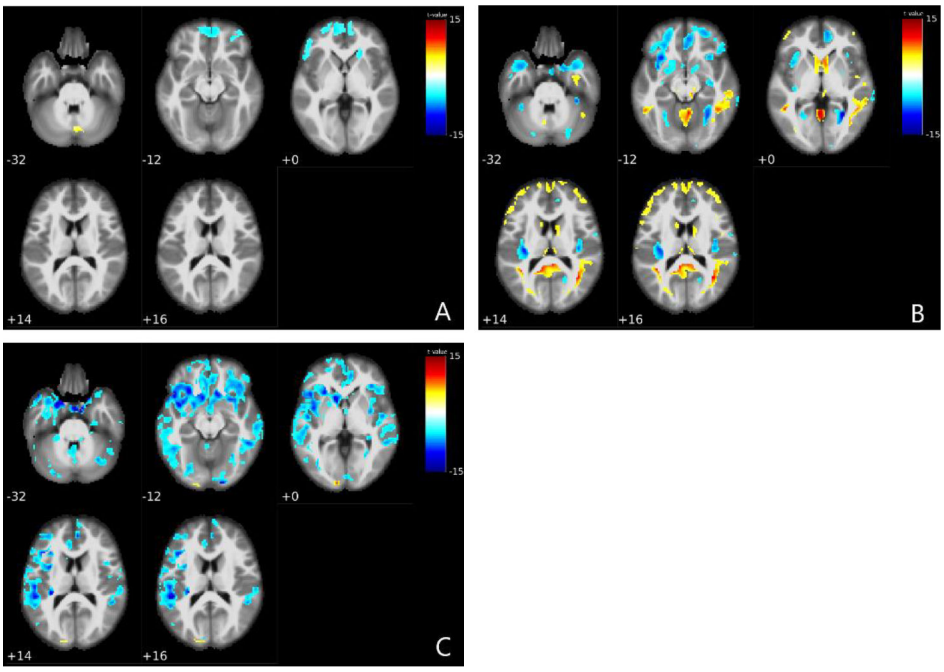

Figure 3:

rCBF difference between MCI and AD identified by three types of ASL data. A) 2D PASL, B) 3D PCASL, C) 3D PASL. Hot color means higher rCBF in MCI; blue color means lower in MCI. The color bar represents statistical significance (t) values. The number underneath each image slice indicate the slice location in the MNI standard brain space.

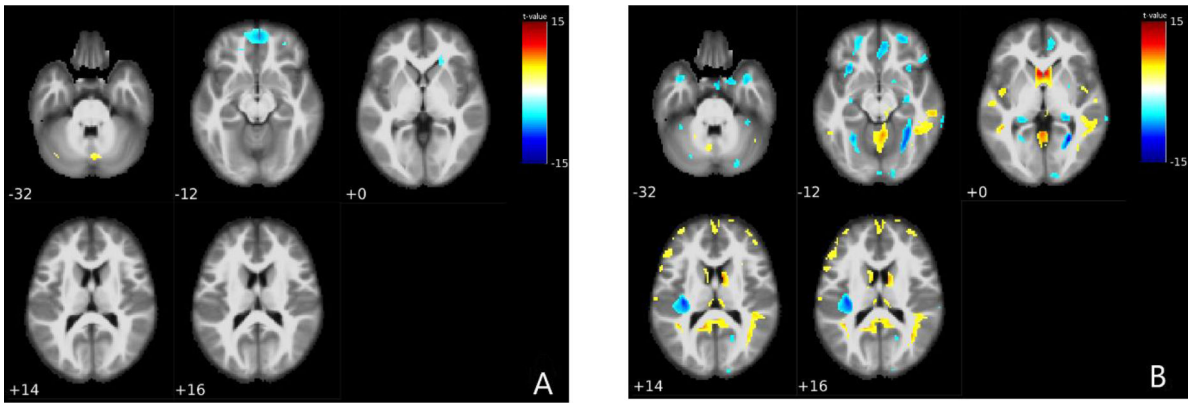

Figure 4:

CBF difference between MCI and AD identified by two types of ASL data. A) 2D PASL, and B) 3D PCASL. Hot color means higher CBF in MCI; blue color means lower in MCI. The color bar represents statistical significance (t) values. The number underneath each image slice indicate the slice location in the MNI standard brain space.

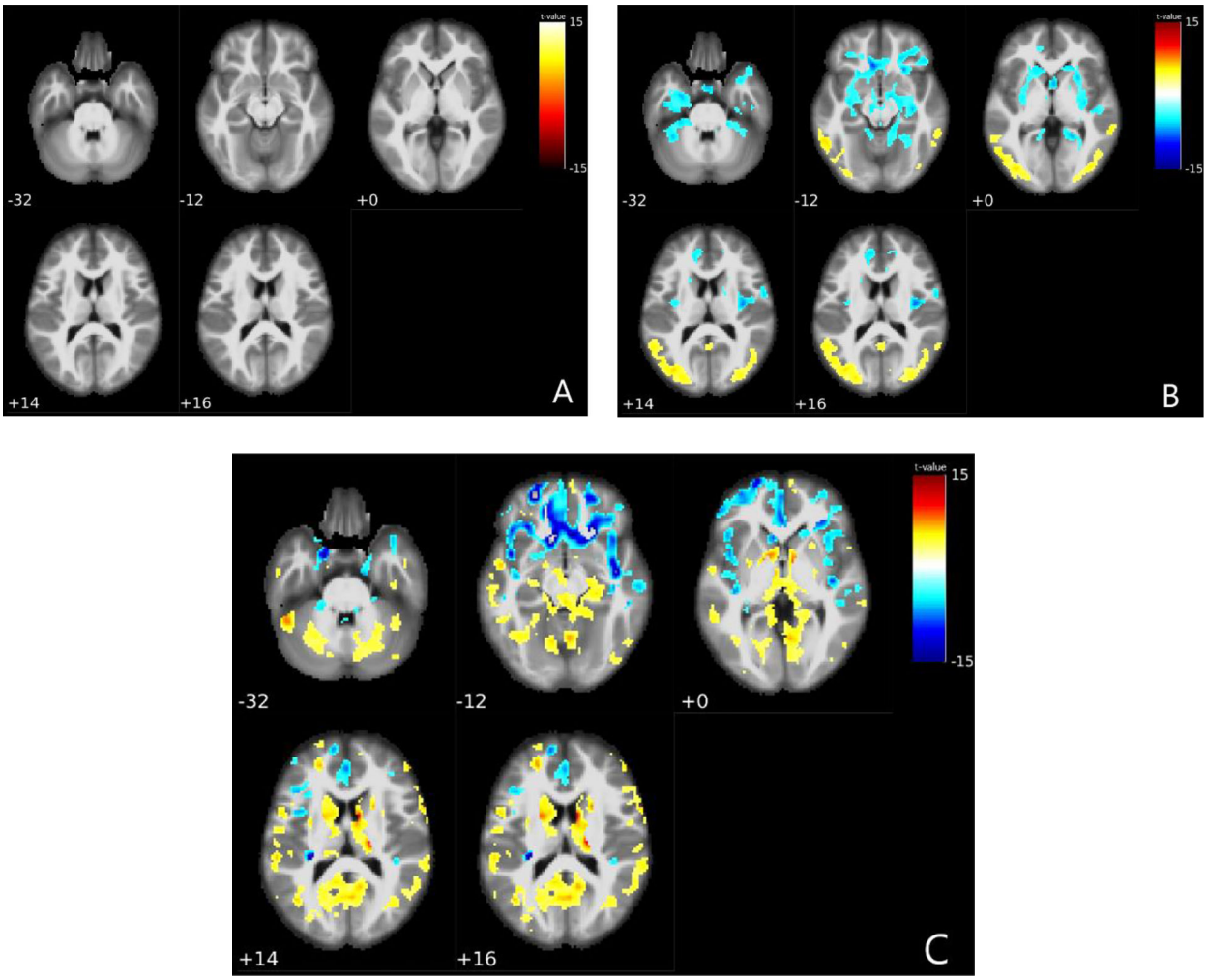

Figure 5:

rCBF difference between NC and AD identified by three types of ASL data. A) 2D PASL, B) 3D PCASL, C) 3D PASL. Hot color means higher rCBF in NC; blue color means lower in NC. The color bar represents statistical significance (t) values. The number underneath each image slice indicate the slice location in the MNI standard brain space.

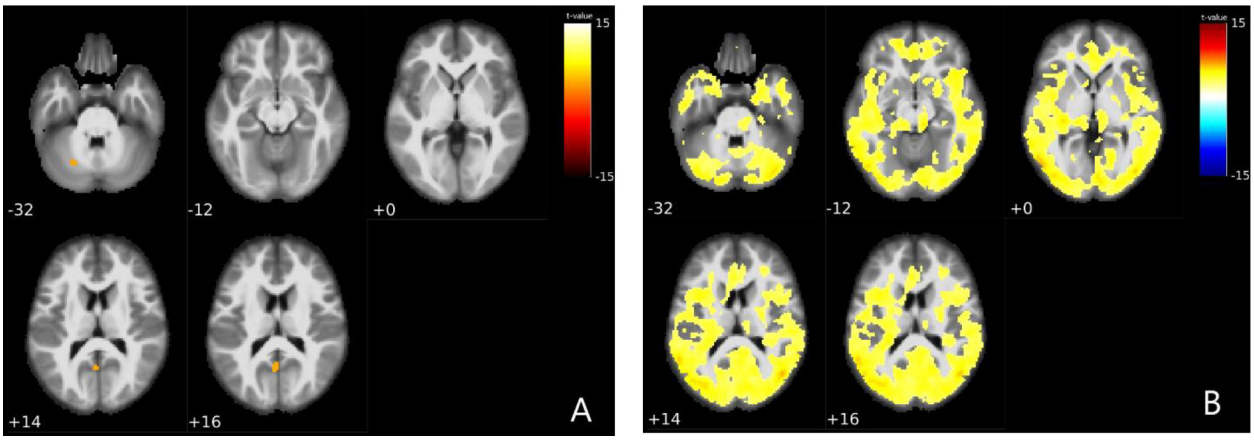

Figure 6:

CBF difference between NC and AD identified by three types of ASL data. A) 2D PASL, B) 3D PCASL. Hot color means higher CBF in NC; blue color means lower in NC. The color bar represents statistical significance (t) values. The number underneath each image slice indicate the slice location in the MNI standard brain space.

TABLE 1:

Demographic and clinical data for subjects who had 2D PASL data

	NC	MCI	AD	F-value	p-value
Number of subjects	25	25	25		
Age (yrs)	72.36 ± 8.19	72.40 ± 8.18	74.52 ± 6.39	2.12	0.12
Sex(F/M)	14/11	11/14	9/16		$<3.1\times10^{-29}$
Education (yrs)	16.6 ± 2.36	16.56 ± 2.71	16.4 (3.1)	0.31	0.73
MMSE	29.04 ± 1.40	27.28 ± 1.81	23.88 ± 2.15	8.97	$<2\times10^{-4}$
LIMM	12.96 ± 2.86	8.10 ± 2.74	4.95 ± 3.13	43.46	$<9.8\times10^{-17}$

TABLE 2:

Demographic and clinical data for subjects who had 3D PCASL data

	NC	MCI	AD	F-value	P-value
Number of subjects	40	25	16		
Age (yrs)	75.05 ± 7.20	74.52 ± 8.59	72.94 ± 7.77	0.42	0.66
Sex(F/M)	18/22	7/18	5/11		$<7.2\times10^{-14}$
Education (yrs)	16.74 ± 1.98	15.87 ± 2.12	15.73 ± 3.08	1.52	0.23
MMSE	29.45 ± 0.76	26.92 ± 1.78	23.68 ± 2.09	4.82	<0.01
LIMM	14.09 ± 2.40	10.44 ± 3.93	6.97 ± 2.05	4.82	<0.01

TABLE 3:

Demographic and clinical data for subjects with 3D PASL data

	NC	MCI	AD	F-value	p-value
Number of subjects	35	25	16		
Age (yrs)	69.86 ± 7.09	72.33 ± 7.90	72.78 ± 9.13	1.17	0.31
Sex(F/M)	20/15	12/13	7/9		$<3.3\times10^{-13}$
Education (yrs)	16.77 ± 2.31	13.32 ± 2.18	14.89 ± 2.17	20.03	$<8.25\times10^{-8}$
MMSE	29.26 ± 1.20	26.20 ±3.05	22.52 ± 3.86	38.27	$<1.82\times10^{-12}$
LIMM	13.50 ± 4.25	7.58 ± 2.58	4.28 ± 2.52	51.48	$<3.28\times10^{-15}$

TABLE 4:

Image Acquisition parameters for 2D PASL, 3D PASL, and 3D PCASL

	2D PASL	**3D PASL / 3D PCASL**
MPRAGE	3D T1, 176 sagittal slices, Flip angle 9^0 TR/TE/TI = 2300/2.98/900 ms FOV:256x240 mm2 Voxel-size:1.1x1.1x1.2 mm3 Bandwidth = 240 Hz/pix	3D T1 TR/TI = 2300/900 ms FOV:208x240x256 mm3 Voxel-size:1.0x1.0x1.0 mm3
ASL	2D PICORE Seq. Q2TIPs TR/TE: 3400/12 ms TI1/TI2 = 700/1900 ms, FOV = 256 mm bandwidth = 2368 Hz/pix, imaging matrix = 64 × 64. does not come with M0	TR/TE: 4885/10.5 ms PLD = 2000 ms Voxel-size:1.9x1.9x4 mm3 FOV = 240x240x160 mm3 3D PCASL comes with M0 3D PASL does not come with M0